Size Reduction of Electromagnetic Bandgap (EBG) Structures with New Geometries and Materials

Yoshitaka Toyota*, A. Ege Engin**, Tae Hong Kim**, Madhavan Swaminathan**, Swapan Bhattacharya**
*Department of Communication Network Engineering, Okayama University
**Packaging Research Center, School of Electrical and Computer Engineering, Georgia Institute of Technology
3-1-1 Tsushima-naka, Okayama, 700-8530 Japan
toyota@cne.okayama-u.ac.jp, engin@ece.gatech.edu

Abstract

Size reduction of an electromagnetic bandgap (EBG) structure with large patches and small branches that connect adjacent patches for a power/ground plane pair is studied. To shrink the dimensions with a high isolation at the frequency of interest, this paper provides two approaches. One is a geometric approach which is to place two narrow slits on each patch. The increase of branch inductance with the long slit successfully decreases the on-set frequency of the stopband without increasing the patch size. The other approach is to use high-K material for a thin dielectric layer. In this case, the size reduction can be predicted according to a scaling law. These approaches are applied together to realize an EBG structure with the entire size of less than 20 mm on a side. It covers the GSM band with sufficient isolation. Through this study, the dispersion-diagram analysis is used to predict the stopband characteristics.

Introduction

In recent mixed-signal systems where digital and RF/analog circuits are densely packed, electromagnetic interference is a critical performance issue. To isolate sensitive RF/analog signals from digital noise, the electromagnetic bandgap (EBG) structure can be used. The EBG structure prevents the propagation of electromagnetic waves within a frequency range, and it is more effective than separated-plane structure [1]. An EBG structure proposed in [2-4] provides excellent isolation of more than 60dB. This EBG structure consists of a patterned power/ground plane pair and requires no additional vias, which are necessary in the EBG structure with the high impedance surface (HIS) [5, 6]. Therefore, standard printed circuit board fabrication technique is easily applicable, which is a cost-effective solution.

Figure 1 shows an example of EBG structures with one-dimensional (1-D) lattice (Fig. 1(a)) and two-dimensional (2-D) lattice (Fig. 1(b)) formed in a power/ground pair. These lattices consist of large metal patches and small metal branches connecting adjacent large patches. This paper focuses on the patches and branches of square shape. The EBG pattern may be applied to either the power plane or the ground plane depending on the design.

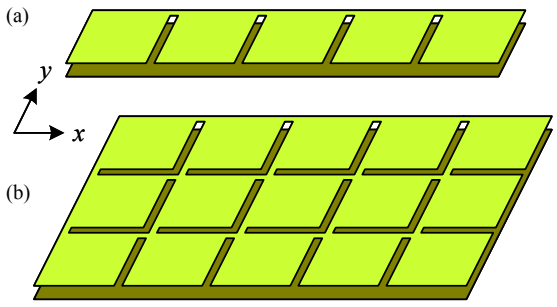

Fig. 1 Examples of EBG lattice combining large square patches with small square branches in a power/ground pair: (a) 1-D EBG lattice; (b) 2-D EBG lattice.

To meet the general demand for more compact wireless devices at the frequency of interest, it is desired to achieve the stopband due to the EBG structure with a patch as small as possible. However, a smaller patch makes the stopband frequency higher since the patch size of this EBG structure determines the on-set frequency of the stopband. To shrink the dimensions of the EBG structure with a high isolation at the frequency of interest, this paper provides two different approaches: introduction of narrow slits into the patch in geometry; and application of high dielectric constant in material.

Through this study, the dispersion-diagram analysis is used to predict the on-set frequency of the stopband. This analysis is available for any EBG structure if a unit cell of the EBG structure is represented as a multi-port network. Since the analysis focuses on the unit cell, it is expected to considerably reduce the calculation time compared with electromagnetic (EM) calculation of the entire EBG structure.

Two approaches for size reduction of the EBG structure

The EBG structure shown in Fig. 1 has passbands and stopbands which alternate with frequency. At lower frequencies, the large patches are predominantly capacitive, whereas the small patches are predominantly inductive. Thus, the EBG structure forms a distributed LC network and hence works as a low-pass filter. At higher frequencies, on the other hand, series and parallel resonances occur alternately in the large patch. Owing to this impedance change caused by the resonances, the EBG structure has passbands and stopbands alternately. Our interest lies in the first stopband above the lowest passband.

As described above, the EBG structure around the first stopband can be considered as a distributed LC network. According to filter theory [7], a cutoff frequency of a low-pass filter with a ladder LC network is defined as $f = 1/\pi\sqrt{LC}$ when a unit network is expressed as a network with a series inductor of L and a shunt capacitor of C. The cutoff frequency corresponds to the on-set frequency of the first stopband in the EBG structure since its unit cell can be roughly regarded as a network consisting of series inductor L and shunt capacitance C at lower frequencies.

The size reduction of the EBG structure must be compatible with an excellent isolation at the frequency of interest. However, a simple size reduction decreases capacitance C and hence a shift of the on-set frequency

towards the higher frequencies occurs as seen in the equation which gives the cutoff frequency of low-pass filter. Therefore, two approaches proposed in the introduction can be restated as follows: the first is to compensate the decrease of C by the increase of L which is caused by introducing narrow slits to the patch; the second is to maintain C of the patch in spite of size reduction.

The first approach of increasing L will be realized by placing two narrow slits with a width of w_s on the patch with a side of a_p as shown in Fig. 2. The narrow slits help to lengthen the one side of the square branch with a side of a_b and hence increase the inductance of the branch. The length of the slit is defined as $L_r a_p$, where L_r is a slit-length ratio which takes a value between 0 and 1.

The other approach corresponds to increasing the dielectric constant ε_r of the dielectric layer between power/ground planes. This will be realized by replacing conventional FR-4 with high-K material. Taking the wavelength in each medium into account, the size reduction factor K_r is given as

$$K_r = \sqrt{\varepsilon_{r,low} / \varepsilon_{r,high}} \ (<1), \qquad (1)$$

where $\varepsilon_{r,\,low}$ and $\varepsilon_{r,\,high}$ are the dielectric constants of FR-4 and high-K material, respectively. Thus, the dimensions of EBG structure with high-K material should be reduced to K_r compared with that of the EBG structure formed with a thin dielectric of FR-4.

In this paper, decreasing the dielectric thickness d is not dealt with because the inductance L is proportional to d and then the product of L and C is independent of d.

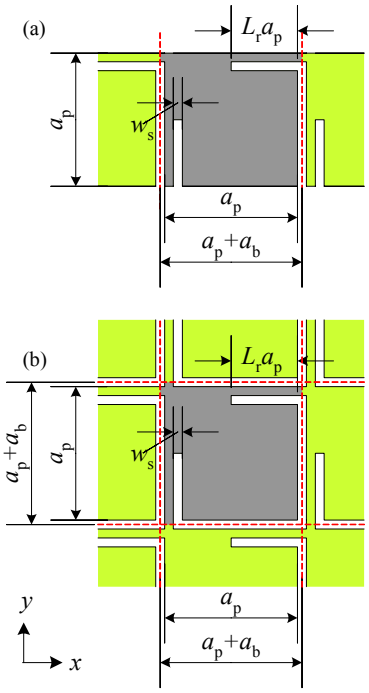

Fig. 2 Unit cells with two narrow slits: (a) 1-D EBG; (b) 2-D EBG. The dashed line indicates the boundary between adjacent unit cells.

Stopband prediction based on dispersion diagram

In this study, the dispersion diagram for an infinitely periodic EBG structure was used to investigate the first stopband of EBG structure. The dispersion diagram is obtained by solving the eigenvalue equation for the infinitely periodic structure. If a unit cell of a 1-D infinitely periodic

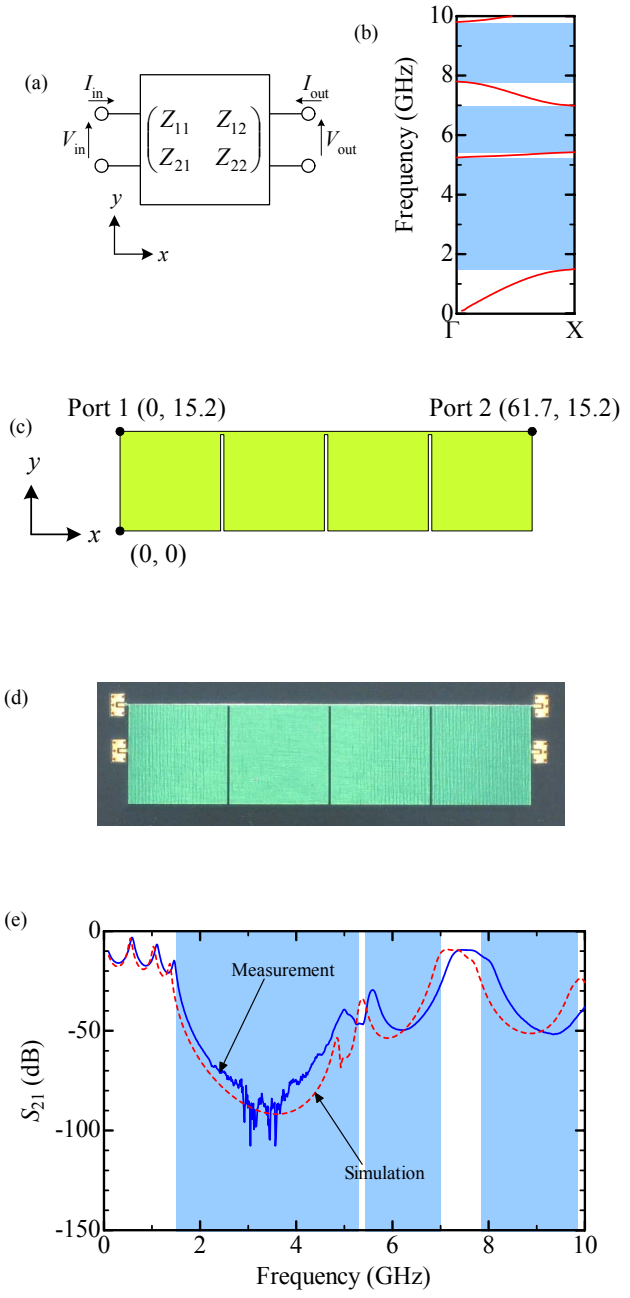

Fig. 3 (a) 1-D unit network represented by the Z parameters; (b) Calculated dispersion diagram of the 1-D EBG unit cell with a_p =15.2 mm, a_b = 0.254 mm, d = 127 μm, and ε_r = 4.0. The colored area shows the stopband of EBG structure; (c) 1-D EBG lattice of 4x1 geometry (unit in mm); (d) Photo of the DUT used for measurement. (e) Comparison of transmission coefficient S_{21} for the 4x1 geometry between the measurement and simulation with Sonnet emCluster. The colored area shows the stopband of EBG structure predicted with the dispersion diagram shown in (b).

structure is represented by the Z parameters Z_{11}, Z_{12} (= Z_{21}), and Z_{22} as shown in Fig. 3(a), the eigenvalue equation is given by

$$\cosh \gamma D = \frac{Z_{11} + Z_{22}}{2Z_{12}}, \qquad (2)$$

where γ and D are the propagation constant for the periodic structure and periodic interval, respectively [8]. In this study, we have $D = a_p + a_b$ as seen in Fig. 2. The eigenvalue equation for a 2-D infinitely periodic structure can be obtained by extending the derivation of (2).

This analysis has the advantage of estimating the stopband of periodic EBG structure by knowing the Z parameters of the unit cell, without any calculations for the entire EBG structure. The Z parameters of a unit cell can be calculated not only by full-wave EM solvers but also by using SPICE models. The latter can be solved more efficiently by applying the Transmission Matrix Method (TMM) [9]. In fact, a comparison of simulation time with a commercial tool, Sonnet, resulted in 70X improvement [10]. Thus, the analysis based on the dispersion diagram enables considerable calculation time reduction.

In order to show that the stopband obtained from dispersion diagram is accurate, the 1-D EBG structure is investigated. The unit cell has the following parameters: a_p = 15.2 mm (600 mils); a_b = 0.254 mm (10 mils); d = 127 μm (5 mils). In calculating the Z parameters of unit cell, we assumed that there are no material losses and the dielectric constant ε_r is 4.0. Figure 3(b) shows the dispersion diagram for this example. In the figure, the colored area indicates the stopband since the plots in the dispersion diagram correspond to wave propagation towards the x-direction. The 1-D EBG structure of the 4x1 geometry shown in Fig. 3(c) was used to evaluate the dispersion-diagram analysis. Figure 3(d) is a photo of a DUT used for measurement. In regards to transmission coefficient S_{21} from Port 1 to Port 2 shown in Fig. 3(c), Fig. 3(e) shows the measured S_{21} (solid curve) together with S_{21} simulated by Sonnet emCluster (dashed curve). In the Sonnet calculation, a dielectric loss of $\tan\delta$ = 0.02 and a copper conductivity of σ_c = 5.8x10^7 S/m were given. The stopband predicted with Fig. 3(b) is superposed on Fig. 3(e). Figure 3(e) indicates that the stopband predicted with the dispersion diagram has a good agreement with the measured and simulated data. In the following discussion, the stopband predicted from the dispersion-diagram analysis will be regarded as the stopband of EBG structure.

Size reduction with narrow slits

In this section, the size reduction due to the application of slits to the patch will be discussed. Adding the slits, the branch becomes a long and narrow rectangle with one side of w_s = 0.254 mm (10 mils) and the other side of $w_s + L_r a_p$. Figure 4 shows the on-set frequency in the first stopband with the slit-length ratio L_r for both 1-D and 2-D EBG structures of the unit cell with a_p = 15.2 mm (600 mils), a_b = 0.254 mm (10 mils), and d = 127 μm (5 mils). As seen in this figure, the on-set frequency decreases with the ratio L_r. This means that the patch with two narrow slits helps to shift the stopband towards the lower frequencies without changing the dimensions of the patch. Or, to put it in another way, a smaller size patch with narrow slits can provide isolation in the same frequency band as a larger size patch without slits.

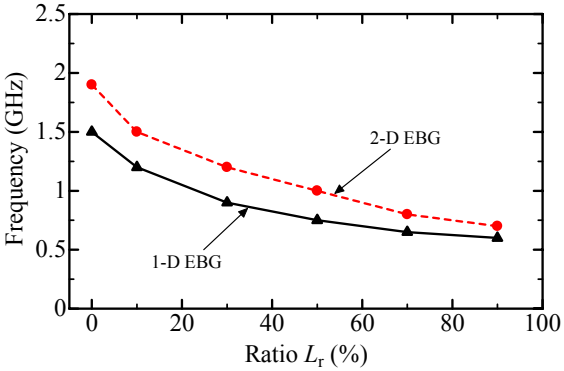

Fig. 4 On-set frequency characteristics with the slit-length ratio L_r.

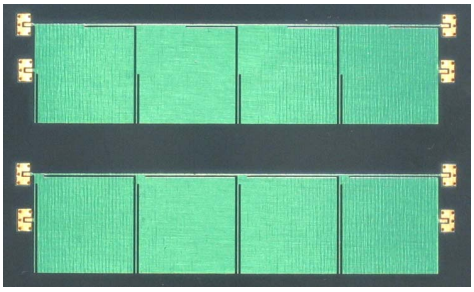

Fig. 5 Photo of DUTs with the 4x1 geometry for L_r = 50% (top) and L_r = 90% (bottom).

To experimentally confirm the on-set frequency shift with the slit length, DUTs with 1-D EBG or 2-D EBG were fabricated.

First, DUTs of 4x1 geometry shown in Fig. 5 were examined. The slit ratios L_r of the DUTs are 50% and 90%. Except for slits, the physical parameters of unit cell are same as those in the previous section. To obtain the electrical properties, the 2-port measurement was carried out with an Agilent 8720ES vector network analyzer (VNA). The port location is same as shown in Fig. 3(c). Figure 6(a) shows the measured transmission coefficient S_{21} in the case of L_r = 0%, 50%, and 90%. The three arrows on top of Fig. 6(a) indicate the on-set frequencies predicted from the dispersion-diagram analysis, and they are the on-set frequencies for L_r = 0%, 50%, and 90% in order from the right. The shift of the first stopband towards the lower frequencies was experimentally observed as predicted. In addition, the isolation of the first stopband is below –60dB, independent of L_r.

Figure 6(b) shows the measured data of input impedance for the same DUTs. The input impedance in the first stopband is as small as approximately several ohms.

Now, the optimum value of the slit-length ratio L_r is considered. As shown in Fig. 4, the on-set frequency gets lower as L_r gets larger. According to the dispersion-diagram analysis, the slits with L_r = 90% provide the lowest on-set

frequency but generate the narrow second passband around 3 GHz. In fact, Fig. 6 shows the degradation of isolation and the increase of input impedance around 3 GHz. In the VNA measurement using ports located in the middle of the patch side shown in Fig. 5, worse, the input impedance reached hundreds ohms around 3GHz. This is considered that the long slit results in quite large inductance of branch. To avoid the quite large input impedance, therefore, the slit-length ratio of 50% is a better choice since the frequency reduction rate for $L_r > 50\%$ is much smaller than that for $L_r < 50\%$.

The dispersion-diagram analysis is suitable to mention the intrinsic stopband of EBG structure as discussed above. It is quite difficult to find narrow passband as seen in Fig. 6 only using the transmission coefficient of the entire EBG structure. For example, Wang *et al.* [11] proposed the EBG unit cell with long L-shaped branches to increase the inductance of branch and decrease the gap between adjacent unit cells. Not only the wide first stopband of 4GHz but the degradation of isolation at 2.5 GHz within the stopband was observed in the transmission coefficient. According to the dispersion-diagram analysis, the degradation is caused by a narrow passband around 2.5 GHz. Therefore, the degradation is considered to be caused by quite large inductance of branch, which is same as described above. Thus, the dispersion-diagram analysis is quite useful for predicting the intrinsic stopband. In order to increase the inductance of branch, in addition, the narrow slits proposed in this paper are better than the L-shaped branch because the gap between the adjacent patches is narrower.

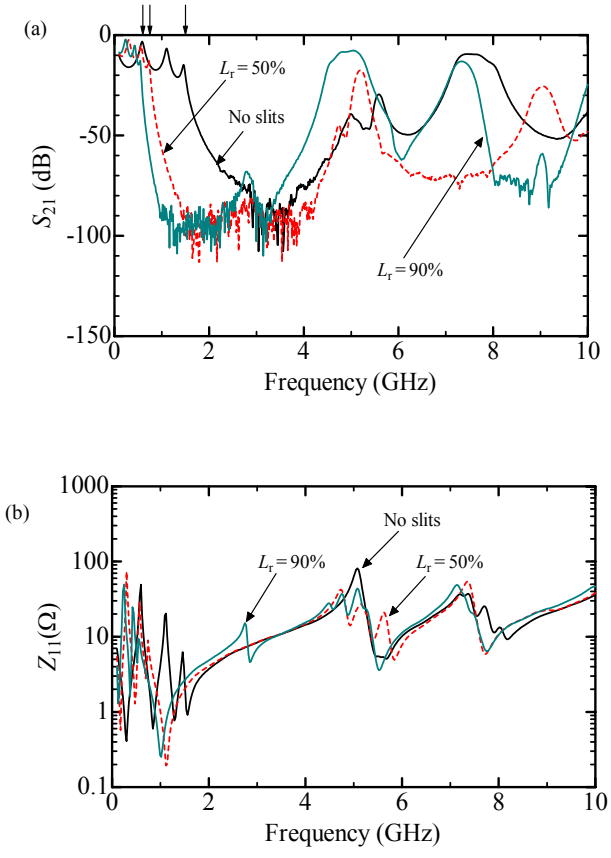

Fig. 6 (a) Measured transmission coefficient S_{21}. The three arrows on the frame show the predicted on-set frequencies for L_r = 0%, 50%, and 90% in order from the right. (b) Input impedance Z_{11} measured at Port 1 shown in Fig. 3(c).

Next, the stopband of the 2-D EBG structure with slits shown in Fig. 7 was investigated. The unit cell has the following parameters: a_p = 15.2 mm (600 mils); a_b = 0.254 mm (10 mils); d = 127 μm (5 mils); w_s = 0.254 mm (10 mils); L_r = 50%. Figure 8(a) shows the 2-D dispersion diagram which is plotted accounting for the Brillouin zone. The colored area of Fig. 8(a) shows complete stopband indicating no wave propagation towards any directions. This complete stopband is regarded as the stopband in 2-D EBG structure. Figure 8(b) shows the measured data of the transmission coefficient S_{21} from Port 1 to Port 2 and to Port 3 shown in Fig. 7(a) together with the colored area which indicates the stopband predicted with the dispersion-diagram analysis. Figure 8(b) shows that the 2-D dispersion-diagram analysis provides a good prediction of the stopband as well as the 1-D analysis. It is also seen that the DUT of 2-D EBG structure with 50% slit length has a good isolation over the stopband.

Size reduction with high-K material

The size reduction of EBG structure should be achieved by replacing conventional FR-4 with high-K material. Since the wavelength in dielectric materials with ε_r is $1/\sqrt{\varepsilon_r}$ times as short as that in the air, the dimensions of EBG structure can be reduced when the dielectric material with a large dielectric constant is used. According to (1), the high-K material with

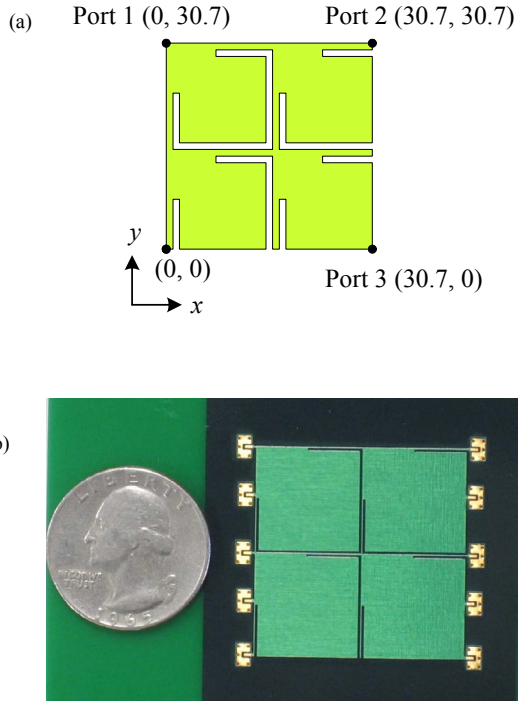

Fig. 7 (a) 2-D EBG structure of 2x2 geometry with a_p = 15.2 mm, a_b = 0.254 mm, d = 127 μm, ε_r = 4.0, w_s = 0.254 mm, and L_r = 50% (unit in mm). (b) Photo of DUT with 2x2 geometry.

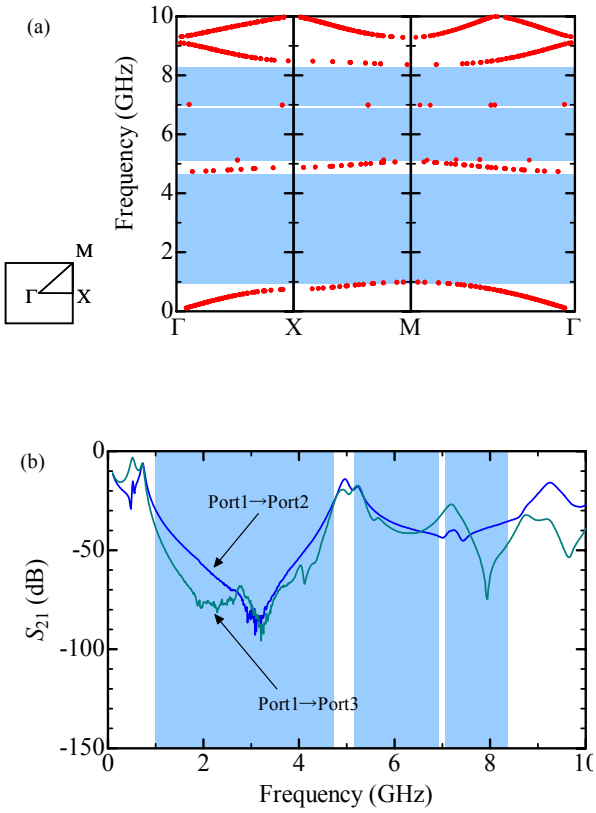

Fig. 8 (a) Calculated dispersion diagram of the 1-D EBG unit cell. (b) Measured transmission coefficient S_{21}. The colored area shows the stopband of EBG structure predicted with the dispersion diagram of (a).

ε_r = 30, which is about 7 times larger than the dielectric constant of FR-4, is expected to reduce the entire size to approximately 40 %. Assuming K_r = 0.4, two pairs of the patch and the branch were chosen as follows: a patch with 15x15 mm and a branch with 1x1 mm (Pattern A); a patch with 6x6 mm and a branch with 0.4x0.4 mm (Pattern B). In the following section, the 3x3 geometry of EBG structure is chosen for discussion. Figure 9 shows a comparison of the entire size of the 3x3 geometry between Pattern A and Pattern B, and the port locations.

First, the first stopband of 2-D EBG structure without slits was examined. Table 1 summarizes the predicted on-set frequencies of the first stopband together with the combination of the dimensions and the dielectric constant. The first two rows have a good agreement of on-set frequency at 1.8 GHz. As for Pattern B with FR-4, on the other hand, the on-set frequency of the first stopband is 2.5 times larger due to the small size and low dielectric constant of 4.6.

Next, Fig. 10 shows the transmission coefficient S_{21} from Port 1 to Port 2 for the 3x3 geometry shown in Fig. 9. Sonnet/emCluster was used for simulation. Two arrows on top of Fig. 10 indicate the on-set frequencies predicted from the dispersion-diagram analysis as shown in Table 1. As shown in Fig. 10, a good isolation in the stopband is observed for high-K material as well. The size reduction due to the high-K material according to the scaling law is realized as expected.

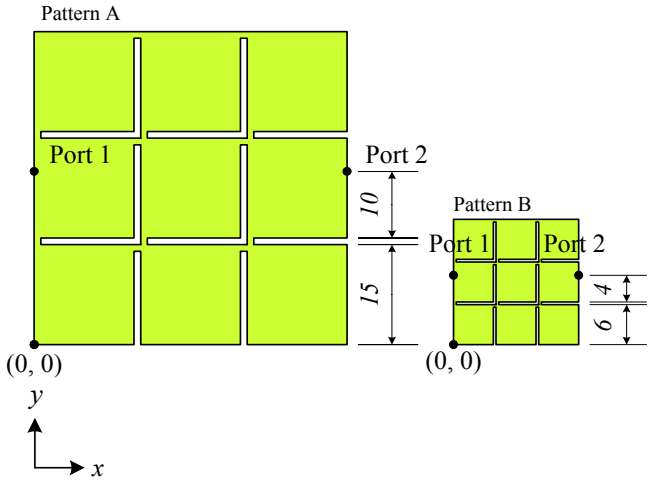

Fig. 9 Comparison of 2-D EBG structures of 3x3 geometry (unit in mm).

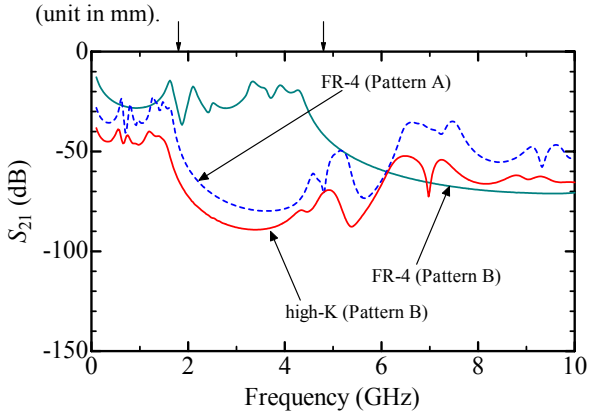

Fig. 10 Calculated transmission coefficient S_{21} for the 2-D EBG structure without slits. The arrows on the frame show the predicted on-set frequencies of 1.8 GHz and 4.8 GHz, as shown in Table 1.

Table 1 Predicted on-set frequencies of the 2-D EBG structure for combinations of the dimensions and the dielectric constant.

Material (ε_r)	Patch (mm)	Branch (mm)	Thickness (μm)	On-set freq. (GHz)
FR-4 (4.6)	15	1	50	1.8
high-K (30)	6	0.4	16	1.8
FR-4 (4.6)	6	0.4	50	4.8

Size reduction with a combination of two approaches

Finally, the EBG unit cell with narrow slits together with the high-K material was examined. Two approaches proposed in this paper are compatible. To examine the isolation as well as the on-set frequency of the first stopband, Sonnet/emCluster simulation was used. Figures 11(a) and 11(b) show the S_{21} data for Pattern A with FR-4 and Pattern B with high-K material, respectively. In this simulation, the slit-length ratio L_r was set to be 50% and the slit width w_s was varied. Since the width of branch is assumed to be same as the slit width, the narrower slit makes the branch narrower.

It is seen from Fig. 11 that the transmission coefficients of both EBG structures are almost same. In addition, the narrow slit and branch improve isolation of the stopband and makes the on-set frequency lower. As a result, the EBG structure with the entire size of 18.8 x 18.8 mm, the dielectric

constant of 30, and the slit width of 0.2 mm can cover the GSM band.

Conclusions

To shrink the EBG dimensions with a high isolation at the frequency of interest, this paper presented two effective approaches: introduction of narrow slits into the patch in geometry; and application of high dielectric constant in material. Each approach was found to contribute to size reduction of EBG structure. By applying these approaches simultaneously, furthermore, an EBG structure which covers the GSM band with sufficient isolation was realized in the entire size of less than 20mm on a side. Through this study, the dispersion-diagram analysis was applied to estimate the stopband of the EBG structure. The on-set frequency predicted from the analysis had a good agreement with that of measured and simulated transmission coefficients.

Acknowledgments

The authors thank Sonnet Software for making emCluster available.

References

1. T. E. Moran, K. L. Virga, G. Aguirre, and J. L. Prince, "Methods to Reduce Radiation From Split Ground Planes in RF and Mixed Signal Packaging Structures," *IEEE Trans. Advanced Packaging*, Vol. 25, No. 3, (2002), pp. 409-416.
2 J. Choi, V. Govind, and M. Swaminathan, "A novel electromagnetic bandgap (EBG) structure for mixed-signal system applications," *Proc. IEEE Radio and Wireless Conf*., Atlanta, GA, Sep. 2004, pp. 243-246.
3 J. Choi, V. Govind, M. Swaminathan, L. Wan, and R. Doraiswami, "Isolation in mixed-signal systems using a novel electromagnetic bandgap (EBG) Structure," *Proc. of IEEE 13th Topical Meeting on Electrical and Performance of Electronic Packaging (EPEP)*, Portland, OR, Oct. 2004, pp. 199-202.
4 T. H. Kim, D. Chung, A. E. Engin, Y. Toyota, M. Swaminathan, "A novel synthesis method for designing electromagnetic band gap (EBG) structures", *Proc. Of the 56th Electromagnetic Components and Technology Conference (ECTC)*, San Diego, CA, May 2006.
5 T. Kamgaing, and O. M. Ramahi, "A novel power plane with integrated simultaneous switching noise mitigation capability using high impedance surface," *IEEE Microwave Wireless Components Lett.*, Vol. 13, No. 1, (2003) pp. 21-23.
6 S. Shahparnia, and O. M. Ramahi, "High-Impedance Electromagnetic Surfaces with a Forbidden Frequency Band", *IEEE Trans. Electromagnetic Compatibility*, Vol. 46, No. 4 (2004), pp. 580-587.
7 D. M. Pozar, Microwave Engineering, 3rd ed. John Wiley & Sons (New Jersey, 2005), Chap. 8.
8 R. E. Collin, Foundations for Microwave Engineering, 2nd ed. McGraw-Hill (New York, 1992), Chap. 8.
9 J. Kim and M. Swaminathan, "Modeling of irregular shaped power distribution planes using transmission matrix method," *IEEE Trans. Advanced Packaging*, Vol. 24, No. 3 (2001), pp. 334-346.
10 A. E. Engin, M. Swaminathan, Y. Toyota, "Finite Difference Modeling of Multiple Planes in Packages," *Proc. 17th International Zurich Symposium on Electromagnetic Compatibility*, Singapore, Mar. 2006.
11 T.-K. Wang, C.-C. Wang, S.-T. Chen, Y.-H. Lin, and T.-L. Wu, "A new frequency selective surface power plane with broad band rejection for simultaneous switching noise on high-speed printed circuit boards", *Proc. 2005 IEEE International Symposium on Electromagnetic Compatibility (EMC2005)*, Chicago, IL, Aug. 2005, pp.917-920.